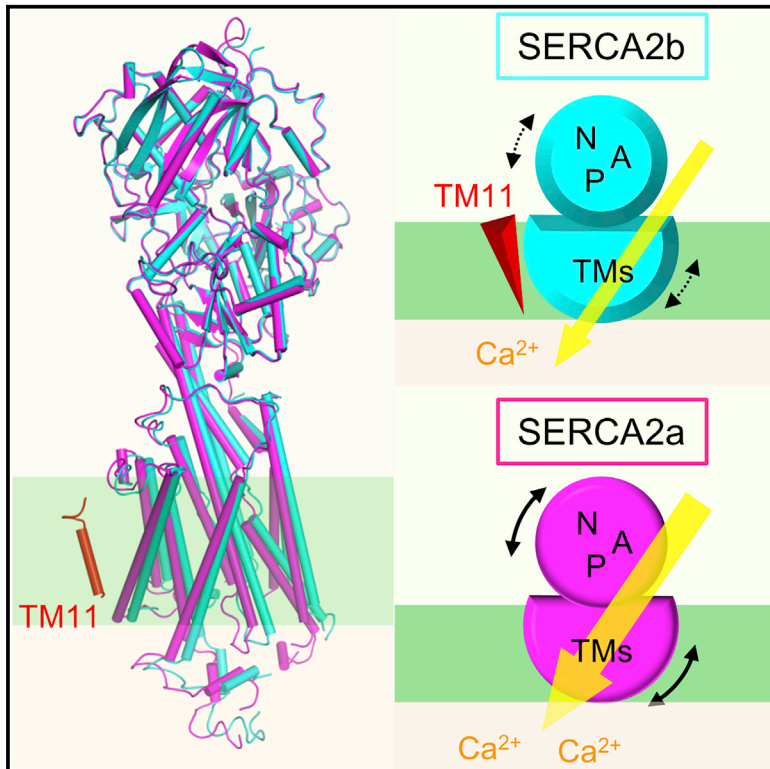


Cell Reports

Structural Basis of Sarco/Endoplasmic Reticulum Ca^{2+} -ATPase 2b Regulation via Transmembrane Helix Interplay

Graphical Abstract



Authors

Michio Inoue, Nanami Sakuta, Satoshi Watanabe, ..., Tomoya Tsukazaki, Kazuhiro Nagata, Kenji Inaba

Correspondence

kinaba@tagen.tohoku.ac.jp

In Brief

Inoue et al. present a crystal structure of human SERCA2b, a ubiquitously expressed Ca^{2+} -ATPase that facilitates Ca^{2+} uptake into the endoplasmic reticulum and thereby plays central roles in intracellular calcium homeostasis. The structural and biochemical analyses clarify molecular mechanisms of SERCA2b regulation via TM helix interplay.

Highlights

- Crystal structure was solved for human SERCA2b and SERCA2a in E1-2 Ca^{2+} -AMPPCP state
- The location and orientation of TM11 helix characteristic of SERCA2b were revealed
- Amino acid residues involved in interaction with TM11 were identified
- Molecular mechanisms of TM11-mediated SERCA2b regulation are proposed



Structural Basis of Sarco/Endoplasmic Reticulum Ca²⁺-ATPase 2b Regulation via Transmembrane Helix Interplay

Michio Inoue,^{1,6} Nanami Sakuta,^{1,6} Satoshi Watanabe,^{1,6} Yuxia Zhang,^{1,6} Kunihito Yoshikaie,² Yoshiki Tanaka,² Ryo Ushioda,^{2,6} Yukinari Kato,⁴ Junichi Takagi,⁵ Tomoya Tsukazaki,² Kazuhiro Nagata,^{3,6} and Kenji Inaba^{1,6,7,*}

¹Institute of Multidisciplinary Research for Advanced Materials, Tohoku University, Sendai 980-8577, Japan

²Graduate School of Biological Sciences, NARA Institute of Science and Technology, Ikoma 630-0192, Japan

³Faculty of Life Sciences, Kyoto Sangyo University, Kyoto 603-8555, Japan

⁴Tohoku University Graduate School of Medicine, Sendai 980-8575, Japan

⁵Institute for Protein Research, Osaka University, Suita 565-0871, Japan

⁶Core Research for Evolutional Science and Technology (CREST), Japan Science and Technology Agency, Saitama, Kawaguchi, Japan

⁷Lead Contact

*Correspondence: kinaba@tagen.tohoku.ac.jp

<https://doi.org/10.1016/j.celrep.2019.03.106>

SUMMARY

Sarco/endoplasmic reticulum (ER) Ca²⁺-ATPase 2b (SERCA2b) is a ubiquitously expressed membrane protein that facilitates Ca²⁺ uptake from the cytosol to the ER. SERCA2b includes a characteristic 11th transmembrane helix (TM11) followed by a luminal tail, but the structural basis of SERCA regulation by these C-terminal segments remains unclear. Here, we determined the crystal structures of SERCA2b and its C-terminal splicing variant SERCA2a, both in the E1-2Ca²⁺-adenylyl methylenediphosphate (AMPPCP) state. Despite discrepancies with the previously reported structural model of SERCA2b, TM11 was found to be located adjacent to TM10 and to interact weakly with a part of the L8/9 loop and the N-terminal end of TM10, thereby inhibiting the SERCA2b catalytic cycle. Accordingly, mutational disruption of the interactions between TM11 and its neighboring residues caused SERCA2b to display SERCA2a-like ATPase activity. We propose that TM11 serves as a key modulator of SERCA2b activity by fine-tuning the intramolecular interactions with other transmembrane regions.

INTRODUCTION

The endoplasmic reticulum (ER) is an essential organelle responsible for Ca²⁺ storage, in which sarco/endoplasmic reticulum Ca²⁺-ATPase (SERCA) imports Ca²⁺ against a huge (>1,000-fold) Ca²⁺ concentration gradient between the ER and the cytosol. Human cells contain 3 different SERCA isoforms divided into 11 splice variants (SERCA1a–1b, -2a–2c, and -3a–3f) (Altshuler et al., 2012). SERCA1a and SERCA2a are expressed mainly in skeletal and cardiac muscle, respectively, while SERCA2b is a ubiquitously expressed house-keeping membrane protein responsible for maintaining Ca²⁺

homeostasis in cells. Residues 1–993 of SERCA2b share an identical amino acid sequence with its splice variant SERCA2a, but the former also possesses a 49-residue C-terminal extension (Campbell et al., 1991) (Figure 1A) that is predicted to contain the 11th transmembrane helix (TM11) and the 12-residue luminal extension (LE) (Campbell et al., 1992). SERCA2a and SERCA1a isoforms, both of which lack TM11 and the C-terminal tail, exhibit higher ATPase activity and lower affinity for Ca²⁺ than SERCA2b (Dode et al., 2003; Verboomen et al., 1992, 1994), indicating a regulatory role for the C-terminal extension in SERCA2b. Accordingly, truncation of the C-terminal 49 residues resulted in a ~2-fold higher turnover rate than wild-type (WT) SERCA2b (Vandecaetsbeek et al., 2009; Verboomen et al., 1994).

A docking model of SERCA2b predicted that TM11 interacts with TM7 and TM10 and that the LE segment binds the groove formed between loops L5/6 and L7/8 (Vandecaetsbeek et al., 2009). Exogenous addition of a synthetic LE peptide (Met1039–Ser1042) to SERCA2a inhibits the ATPase activity and increases the apparent Ca²⁺ affinity, possibly by stabilizing the Ca²⁺-bound E1-2Ca²⁺ state, suggesting that the LE segment serves as a functional modulator of SERCA2b (Vandecaetsbeek et al., 2009). Moreover, co-reconstitution of a synthetic TM11 peptide (Gly1013–Tyr1030) with SERCA1a has a similar functional effect (lower V_{max} and higher Ca²⁺ affinity) to that of LE (Gorski et al., 2012). However, the molecular mechanisms underpinning TM11-mediated SERCA2b regulation remain poorly understood due to a lack of structural information on SERCA2b.

Herein, we present crystal structures of human SERCA2b and SERCA2a, both in the E1-2Ca²⁺-adenylyl methylenediphosphate (AMPPCP) state (Figure 1B). While crystal structures were recently released for E2-AIF₄⁻ and E1-2Ca²⁺-AMPPCP forms of SERCA2a from pig ventricular muscle (Sitsel et al., 2019), we report on the crystal structure of SERCA2b. The crystal structure, in combination with anomalous signal analysis using the single-wavelength anomalous dispersion (SAD) dataset of selenomethionine (SeMet)-labeled SERCA2b, revealed that despite discrepancies with the previously predicted model, TM11 is



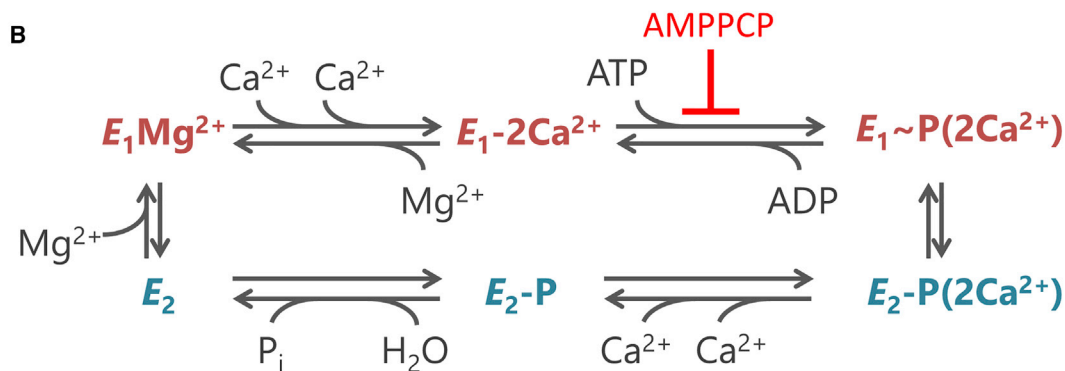
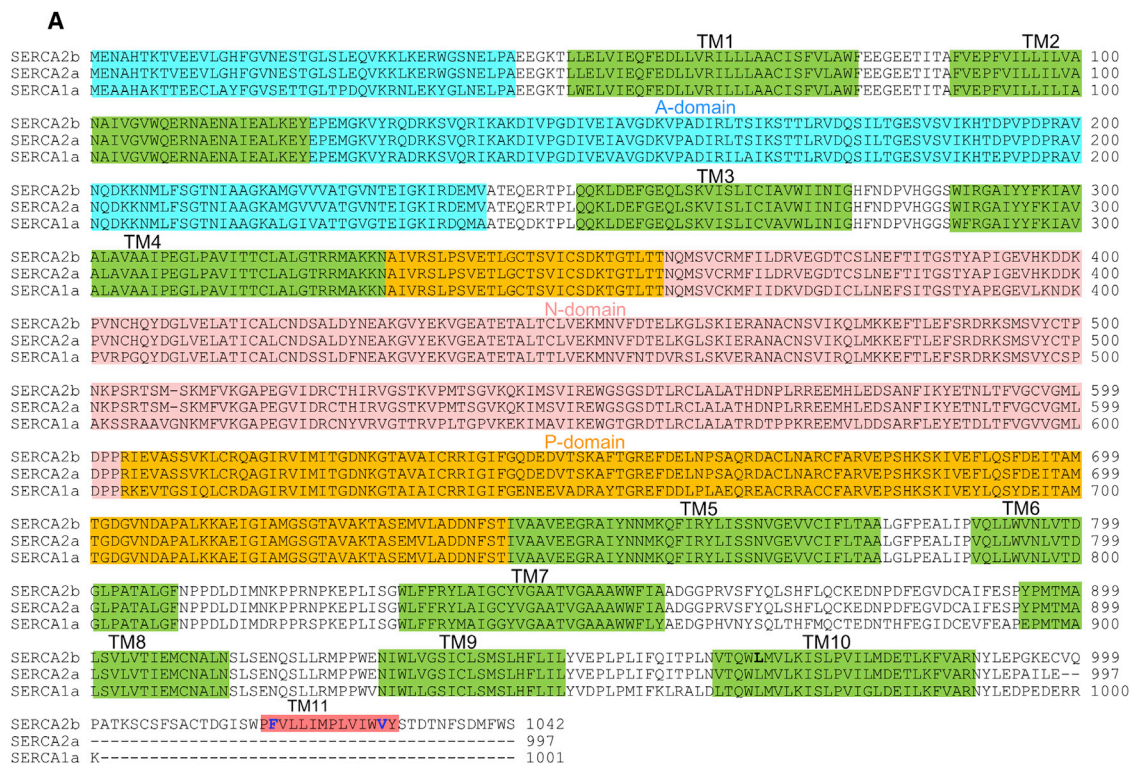


Figure 1. Alignment of the Amino Acid Sequences of Human SERCA Family Members and Catalytic Cycle Exerted by SERCA Family Enzymes

(A) Transmembrane helices TM1–TM10 and TM11 are shown in green and red, respectively. Cytosolic A, N, and P domains are shown in cyan, salmon pink, and orange, respectively. Residues Phe1018 and Val1029 are blue.

(B) Key states generated along the ATP-driven Ca^{2+} pump cycle of SERCA. Note that AMPPCP, a non-hydrolyzable ATP analog, traps the Ca^{2+} -bound state of SERCA to generate the $E_1-2\text{Ca}^{2+}$ -AMPPCP state.

located adjacent to TM10 and does not interact with TM7; instead, the N-terminal and C-terminal ends of TM11 interact with a part of the L8/9 loop and TM10, respectively. Structure-based biochemical studies demonstrated that the functional properties of SERCA2b were significantly affected by the mutations of TM11 residues interacting with the L8/9 loop or TM10. We propose that TM11 serves to fine-tune the turnover rate and Ca^{2+} affinity of SERCA2b through the interplay with other TM regions.

RESULTS AND DISCUSSION

Overall Structures of SERCA2b and SERCA2a

We developed human stable cell lines expressing recombinant human SERCA2b and SERCA2a with an N-terminal dodecapeptide PA-tag (GVAMPGAEDDVV) using the PiggyBac Cuate Switch Inducible system. For stable expression of SERCA2b or SERCA2a, HEK293T cells harboring either one of the SERCA2 genes and the promoter sequence transposed

Table 1. X-Ray Diffraction Data Collection and Refinement Statistics

	SERCA2b	SERCA2a	SeMet-Labeled SERCA2b
Data Collection			
Beamline	SPring-8 BL32XU	SPring-8 BL32XU	SPring-8 BL32XU
Wavelength	1.000	1.000	0.9780
Space group	<i>P</i> 2 ₁ 2 ₁ 2	<i>P</i> 2 ₁ 2 ₁ 2	<i>P</i> 2 ₁ 2 ₁ 2
Cell Dimensions			
a, b, c (Å)	165.08, 84.64, 118.83	165.58, 84.36, 122.19	165.31, 84.87, 121.22
Oscillation × No. crystals	5° × 21, 10° × 25	180° × 1	10° × 42
Resolution (Å) ^a	48.2–3.45 (3.57–3.45)	49.48–3.20 (3.31–3.20)	49.48–5.5 (5.70–5.50)
Completeness (%) ^a	93.7 (77.0)	100 (99.9)	99.1 (99.7)
Redundancy ^a	8.9 (5.1)	6.6 (6.6)	14.0 (14.6)
I/σ (I) ^a	4.7 (1.8)	4.7 (1.3)	4.2 (1.3)
R _{meas} (%) ^{a,b}	33.8 (91.7)	26.4 (147)	44.6 (304)
CC _{1/2} ^a	0.963 (0.511)	0.999 (0.524)	0.660 (0.404)
Refinement Statistics			
Resolution (Å)	48.2–3.45	49.48–3.20	–
R _{work} /R _{free} (%) ^{c,d}	24.9/30.8	21.1/25.6	–
RMSDs			
Bond lengths (Å)	0.007	0.010	–
Bond angles (°)	0.726	0.736	–
Ramachandran Plot			
Favored (%)	94.0	94.0	–
Allowed (%)	6.0	6.0	–
Outliers (%)	0.0	0.0	–

^aValues in parentheses are for the highest-resolution shell.

^bR_{meas} = $\sum_{hkl} \{n/[n-1]\}^{1/2} \sum_i |I_i(hkl) - \langle I(hkl) \rangle| / \sum_{hkl} \sum_i I_i(hkl)$, where $I_i(hkl)$ is the i th observed intensity and $\langle I(hkl) \rangle$ is the average intensity from multiple observations.

^cR_{work} = $\sum |F_o - F_c| / \sum |F_o|$, where F_o and F_c are observed and calculated structure factors, respectively.

^dR_{free} is R factor for a selected subset (5%) of randomly chosen reflections that were omitted in prior refinement calculations.

onto the chromosomes were established through selection by repeated passage in the presence of 10 μg/mL puromycin. Recombinant SERCA2b and SERCA2a were overexpressed using cumate induction (Ushioda et al., 2016) and purified by the established methodology for rapid high-yield purification using the high-affinity antibody NZ-1 (Fuji et al., 2016), followed by size-exclusion chromatography (Figures S1A and S1B). SERCA2a and SERCA2b fully purified in the presence of 1 mM DTT were obtained with a yield of 0.6–1 mg/L culture medium. SERCA2b and SERCA2a were crystallized in complex with Ca²⁺ and AMPPCP, a non-hydrolyzable ATP analog, using the lipidic cubic phase (LCP) method (Figure S1C). X-ray diffraction images of SERCA2b (Figure S1D) were collected from >10 microcrystals, and images of SERCA2a were collected from a single crystal, at SPring-8 beamline BL32XU, and refined to 3.45 and 3.2 Å resolution, respectively (Table 1). Phases were determined by molecular replacement using a previously published crystal structure of AMPPCP-bound SERCA1a (PDB: 1T5S) as a search model.

In both SERCA2b and SERCA2a, clear electron density was observed for the cytosolic A, N, and P domains, and the 10 TM helices (Figure 2A; Videos S1 and S2), allowing model building of

their overall structures (Figure 2B). The locations of the 3 cytosolic domains and the arrangement of TM1–TM10 are almost identical to those previously reported for AMPPCP-bound SERCA1a (Sørensen et al., 2004; Toyoshima and Mizutani, 2004). The modes of ATP binding and calcium coordination in SERCA2b and SERCA2a are also similar to those in SERCA1a, suggesting common mechanisms of ATP hydrolysis and Ca²⁺ transport among the SERCA family members (Figures 1B, S2, and S3). In agreement with the use of reduced forms of SERCA2b and SERCA2a in crystallization, the electron density map of the L7/8 loop indicated that both Cys875 and Cys887 were in reduced form (Figure S4). Enzymatic assays showed that the ATPase activity of SERCA2b reconstituted into liposome was ~2-fold lower than that of SERCA2a (Figure S1E), as reported previously (Vandecaetsbeek et al., 2009). Thus, our SERCA2 preparations retained their intrinsic activities.

Modeling and Physical Location of TM11

Significant electron density was visible adjacent to TM10 in SERCA2b, but not in SERCA2a (Figures 2A and 2B; Videos S1 and S2), indicating that it is derived from TM11 and is characteristic of SERCA2b. To further corroborate our assignment

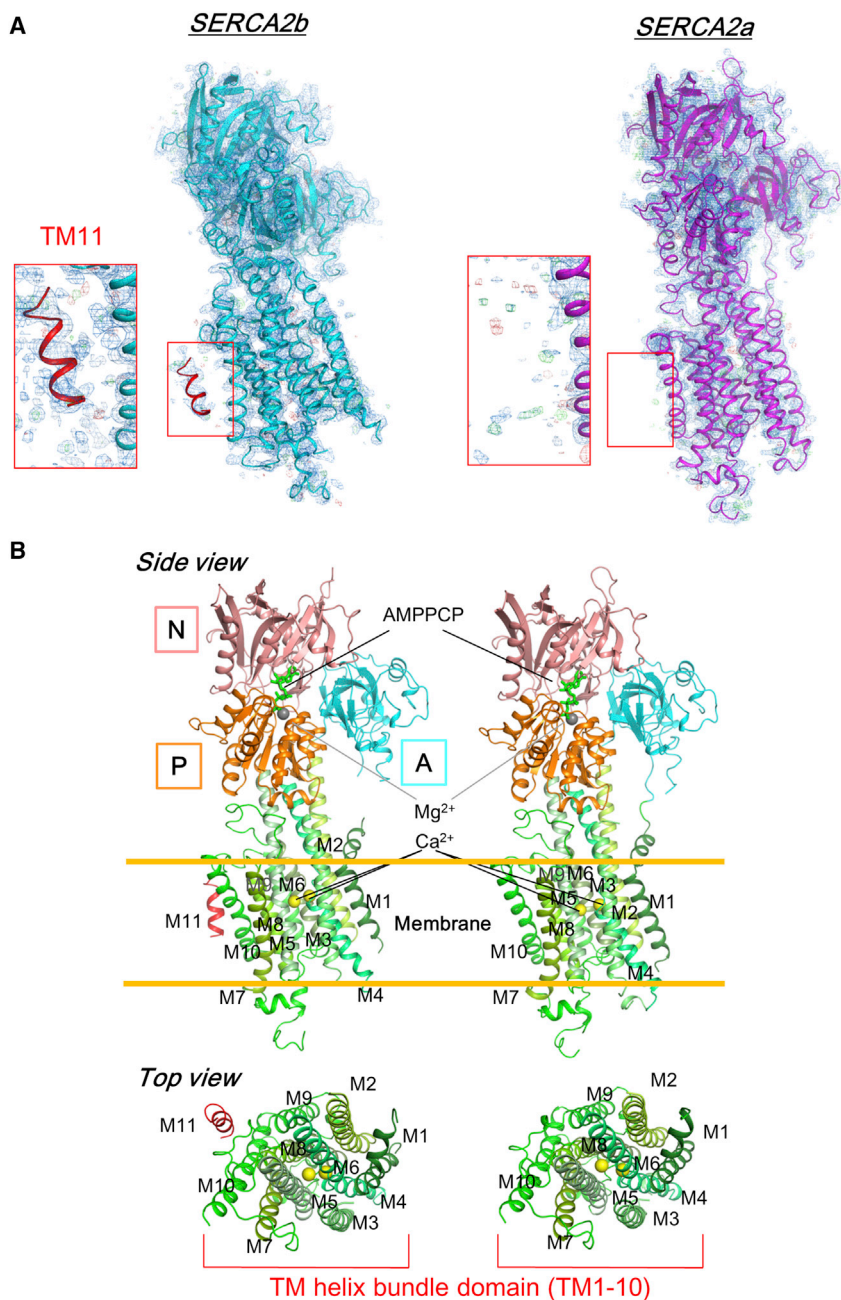


Figure 2. Overall Structures of SERCA2b and SERCA2a in the E1-2Ca²⁺-AMPPCP State

(A) Electron density maps of SERCA2b (left) and SERCA2a (right). 2Fo-Fc maps at the 1.0 σ contour level are shown as blue mesh. The insets show enlarged views of the electron density map in the vicinity of TM10 in SERCA2b (left) and SERCA2a (right). Green and red meshes display positive and negative Fo-Fc maps, respectively, at the 3.0 σ contour level. The C α traces of SERCA2b and SERCA2a modeled based on the 2Fo-Fc maps are shown in ribbon representation.

(B) Crystal structures of SERCA2b and SERCA2a in the E1-2Ca²⁺-AMPPCP state shown in ribbon representation. Cytosolic A, N, and P domains are shown in cyan, salmon pink, and orange, respectively. TM11 (numbered M11) and the transmembrane (TM) helix bundle domain composed of TM1-TM10 (numbered M1-M10) are red and green, respectively. Green sticks in the cytosolic domains denote bound AMPPCP, while yellow and gray spheres represent bound Ca²⁺ and Mg²⁺ ions, respectively. The lower ribbon diagrams show the top view of TM helices from the cytosol.

N- and C-terminal ends of TM11 were found to interact with a part of the L8/9 loop and the ER luminal end of TM10, respectively; Trp927 (L8/9) forms van der Waals contacts with Phe1018 (TM11), while Val1029 (TM11) is surrounded by Leu967, Leu970, and Lys971 (TM10; Figure 3C).

The TM11 region has high B-factor values (135–186 Å²), suggesting its fluctuating property and/or partially disordered helical conformation (Figure 3D). In support of this, the electron density map of SERCA2b at 1.5–2.0 σ counter levels (Figure S5) showed that similar to the L7/8 and L9/10 loops, the TM11 region had fragmented electron density with lower intensity compared to the other TM helices. Accordingly, TM11 is significantly isolated from the TM helix bundle domain, generating a cavity with a volume of >35 Å³ between TM10 and TM11 and a distance of

of TM11, we crystallized SeMet-substituted recombinant SERCA2b and collected a diffraction dataset at the Se K-edge wavelength (0.9780 Å). An anomalous difference Fourier map contoured at 3 σ identified 20 of the 32 selenium sites (Figure 3A). Of particular note, a significant anomalous peak (4.0 σ) was observed close to the putative TM11 backbone, likely derived from Met1023 located in TM11 (Figure 3B). Based on this anomalous peak and the 2Fo-Fc map at 3.45 Å, we modeled the F1018–Y1030 segment of the TM11 helix (Figures 3B and 3C), as previously performed on disulfide bond formation protein B (DsbB), a membranous sulfhydryl oxidase from *Escherichia coli* (Inaba et al., 2006, 2009). Consequently, the

13.7 Å between the C α atoms of Ile977 and Met1023 (Figure 3E). No electron density higher than the 0.4 σ contour level was observed in this cavity, suggesting that there are few, if any, tightly bound phospholipids that intervene between these 2 TM helices. Electron density is missing also for the L10/11 loop and the ER luminal tail following TM11 (Figure 1A). It is likely that these 2 regions are even more fluctuating and/or disordered than TM11. Thus, TM11 and the subsequent tail appear to engage in only limited interactions with other TM regions of SERCA2b. The present finding tempts us to speculate that TM11 may be readily released from the TM helix bundle domain in other intermediate states. It will be interesting to explore

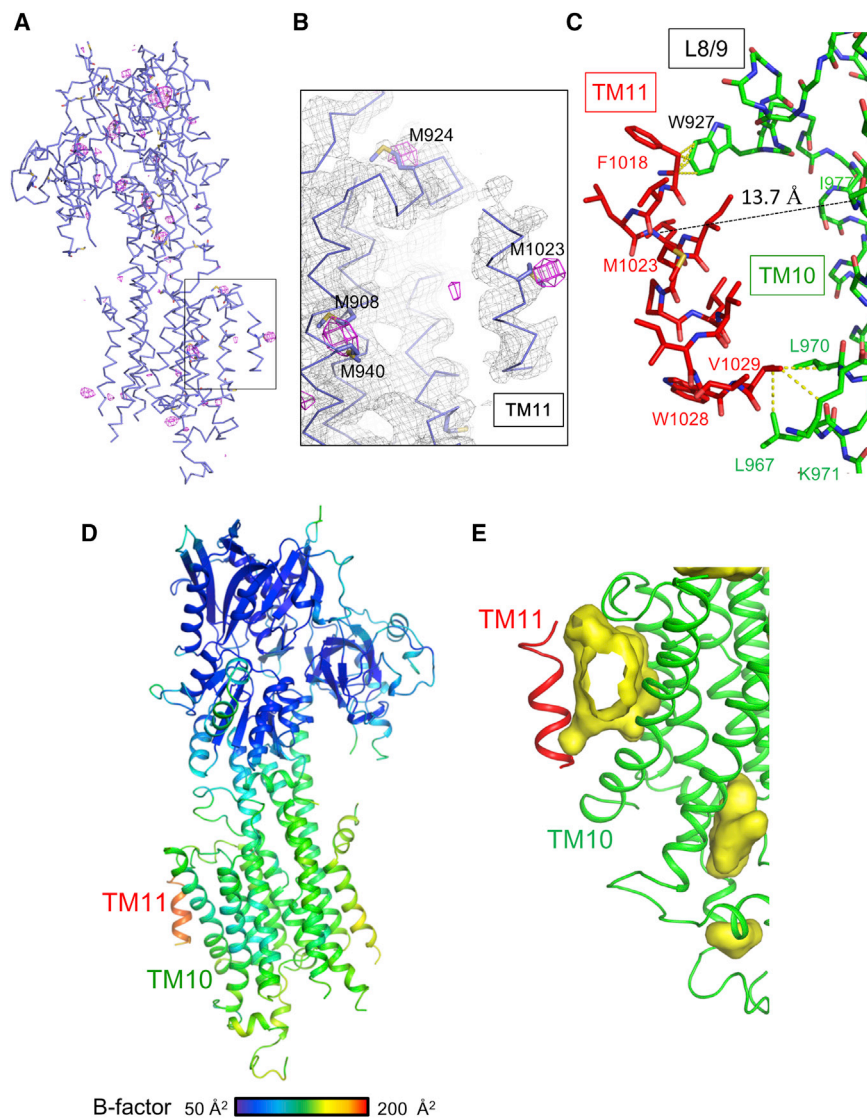


Figure 3. Structural Modeling and Location of TM11 and Its Interactions with Neighboring Residues in SERCA2b

(A) Anomalous difference Fourier map at 6 Å resolution, contoured at 3 σ (magenta mesh). The map was calculated using the dataset from SeMet-labeled SERCA2b crystals. Methionine residues in SERCA2b are shown in stick representation.

(B) Close-up view of the vicinity of TM11 in SERCA2b (black box in 2A). The C α trace of TM11 is superimposed on a 2Fo-Fc map contoured at 1.0 σ (gray). The anomalous difference Fourier map contoured at 3 σ is also shown in magenta, indicating an anomalous peak from SeMet1023 on TM11.

(C) Close-up view of the intramolecular interactions of TM11 with loops L8/9 and TM10 in SERCA2b. The side chains of TM11 and the residues involved in interactions with TM11 are shown as a stick model. Yellow dotted lines indicate pairs of carbon atoms (within 4 Å distance) between hydrophobic side chains present in L8/9, TM10, and TM11.

(D) B-factor distribution of SERCA2b. Residues with B factors between 50 and 200 Å² are indicated by rainbow coloring.

(E) Cavities formed in the TM region of SERCA2b. TM helices of SERCA2b are shown in ribbon representation. Cavities >35 Å³ in the TM region of SERCA2b are visualized as a set of intersecting yellow spheres.

whether TM11 serves to fine-tune the SERCA2b activity through the association with or release from the TM helix bundle domain to maintain the Ca²⁺ homeostasis in the ER (see also the following sections).

Roles of TM11 in SERCA2b Regulation

To quantify the specific activities of SERCA2b and SERCA2a in the membrane-embedded state, we first prepared microsomes of HEK293T cells overexpressing WT SERCA2b and SERCA2a. In agreement with previous results obtained using microsomes of COS cells overexpressing SERCA2a or SERCA2b (Vandecastels et al., 2009), the V_{\max} value of SERCA2b ($1.8 \times 10^2 \text{ min}^{-1}$) was nearly 2.3-fold lower than that of SERCA2a ($4.2 \times 10^2 \text{ min}^{-1}$), while the K_d values for Ca²⁺ binding to SERCA2b and SERCA2a were 0.21 and 0.35 μM , respectively (Figure 4; Table S1). Thus, SERCA2b displayed compromised ATPase activity and increased apparent affinity for Ca²⁺ compared with SERCA2a, implying that TM11 and the subsequent luminal

tail, which are characteristic of SERCA2b, serve as an intramolecular uncompetitive inhibitor. To explore the functional roles of the intramolecular interactions between TM11 and its neighboring residues, and thereby verify the actual occurrence of the interactions, Phe1018 and Val1029 on TM11 were simultaneously mutated to glycine, and the ATPase activity of the resultant mutant (F1018G/V1029G) was measured at various Ca²⁺ concentrations. Microsomal SERCA2b F1018G/V1029G displayed a ~ 1.7 -fold higher V_{\max} value and ~ 1.5 -fold lower affinity for Ca²⁺ than microsomal SERCA2b WT (Figure 4). Thus, disruption of the interactions between TM11 and its neighboring TM regions caused the catalytic turnover rate and Ca²⁺-binding affinity of SERCA2b to resemble those of SERCA2a. Meanwhile, neither of the single mutations F1018G or V1029G greatly affected the ATPase activity of SERCA2b, suggesting that formation of either one of the interactions is sufficient for the TM11-mediated SERCA2b regulation. Collectively, the TM11-involved interactions identified in this crystallographic study play a critical role in regulating the SERCA2b activity.

In this context, Mikkelsen et al. (2018) demonstrated that either the mutation of Glu917, a residue located in the L8/9 loop, or of Arg835, a TM7 residue hydrogen bonded to Glu917, abrogated the inhibitory effect of TM11. It was inferred that the specific interactions between the L8/9 loop and TM7 may be

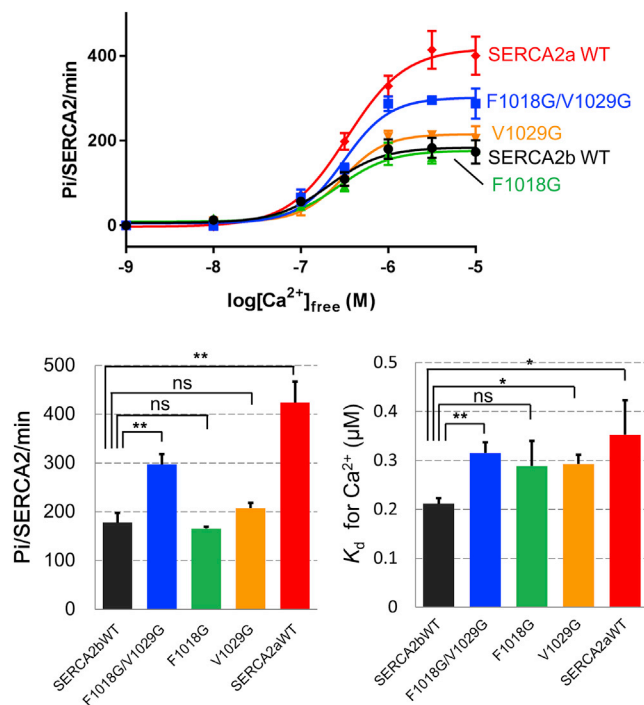


Figure 4. Regulatory Roles of TM11 and Its Interactions with Neighboring Residues in the SERCA2b ATPase Cycle

ATPase activities of microsomal SERCA2b and SERCA2a. The specific activities of SERCA2b WT (black), F1018G/V1029G (blue), F1018G (green), V1029G (orange), and SERCA2a WT (red) are plotted as a function of Ca^{2+} concentration. Bar graphs indicate the maximal turnover rate of the ATPase activity (V_{max} ; left) and the Ca^{2+} -binding affinity (K_d for Ca^{2+} ; right) of SERCA2b WT, its mutants, and SERCA2a WT. Results presented in graphs are means \pm SD of 3 independent experiments. ns, not significant; * $p < 0.05$ and ** $p < 0.005$.

involved in regulating the position of TM11 and its interactions with the surrounding regions. However, the present crystallographic study reveals that TM11 is located on the opposite side to TM7, close to TM10, and makes no direct contact with TM7 (Figure 1B). We surmise that mutational disruption of the Arg835 (TM7)-Glu917 (L8/9) interaction could greatly alter the L8/9 conformation, thereby diminishing interactions between L8/9 and TM11 and hence reducing inhibition by TM11.

Different Binding Sites for TM11 and Phospholamban and Sarcolipin Proteins in SERCA Family Members

It is well known that SERCA2a and SERCA1a are regulated by the small single-spanning membrane protein phospholamban (PLB) and its homologous protein sarcolipin (SLN) (Hughes et al., 1994; Odermatt et al., 1998). Similar to SERCA2a and SERCA1a, PLB and SLN are abundant in cardiac and skeletal muscle, respectively, whereas SERCA2b is expressed ubiquitously (Burk et al., 1989). The crystal structure of SERCA1a in complex with SLN demonstrated that SLN binds to the TM groove formed by TM2, TM4, TM6, and TM9 (Figure 5A) (Toyoshima et al., 2013; Winther et al., 2013). More recently, a transmembrane micropeptide, another-regulin (ALN), which is expressed ubiquitously and shares key amino acids with PLB and SLN, was identified to inhibit

the Ca^{2+} pump activity of SERCA2b (Anderson et al., 2016). The competition assay for binding to SERCA2b suggested that ALN interacts with the same region of the Ca^{2+} -ATPase as PLB and SLN.

The present study revealed that TM11 is located at a completely different site from those micropeptides, suggesting that TM11 regulates SERCA activity in a different manner (for more details, see the following 2 sections). PLB and SLN are reported to bind and preferentially stabilize the Ca^{2+} -free E2 state and/or the E1- Mg^{2+} state before Ca^{2+} binding, thereby inhibiting the transition to the E1- $2Ca^{2+}$ state (MacLennan and Kranias, 2003; Toyoshima et al., 2003, 2013; Winther et al., 2013). In this context, SLN contributes to muscle-based thermogenesis in mammalian cells by uncoupling SERCA-mediated ATP hydrolysis from Ca^{2+} transport (Bal et al., 2012; Ikeda et al., 2017). Previous studies showed that TM11 is critical for low rates of the E2P dephosphorylation step, E2P to E2, and the conformational transition of the dephosphoenzyme, E2 to E1 (Gorski et al., 2012), whereas the subsequent LE region prevents the E1P to E2P transition, independent of TM11 (Clausen et al., 2012; Dode et al., 2003). Thus, TM11 and the LE region likely inhibit the catalytic cycle of SERCA2b in different ways, while their possible roles in the exothermic activity of SERCA2b remains to be explored.

Similar Binding Sites of TM11 in SERCA2b and the TM Helix of Neuroplastin in PII-type ATPase-1

Neuroplastin (NPTN) and Basigin, members of the immunoglobulin (Ig) superfamily with a single TM helix, have recently been identified as obligatory auxiliary subunits of the plasma membrane Ca^{2+} ATPase (PMCA) (Schmidt et al., 2017). PMCA proteins belong to the PII-type ATPase family, like SERCA proteins, and endogenously form a heterotetramer involving NPTN or Basigin to fulfill the Ca^{2+} transport activity. The single TM helix of NPTN or Basigin plays particular roles in stabilizing and trafficking the PMCA complexes (Schmidt et al., 2017). The latest study revealed the cryo-EM structure of PMCA1 in complex with NPTN (Gong et al., 2018), in which PMCA1 assumes a conformation similar to an E1- Mg^{2+} state, a transient state from E2 to E1- $2Ca^{2+}$ states. The TM helix and the Ig domain of NPTN were found to interact with TM10 and the L7/8 loop of PMCA1, respectively. The superposition of SERCA2b with the PMCA1-NPTN complex indicates that TM11 in SERCA2b is located at a similar position to the NPTN TM helix in the PMCA1-NPTN complex, even though these 2 TM helices are arranged in different angles with respect to the TM helix bundle domains (Figure 5B). The NPTN TM helix (21 residues), which is longer than SERCA2b TM11 (13 residues), interacts tightly with TM10 of PMCA1 (Figure S6A). The contact area between the NPTN TM helix and PMCA1 TM10 is 259.1 \AA^2 , while that between TM11 and TM10 in SERCA2b is 80.5 \AA^2 . Accordingly, the NPTN TM helix region has low B-factor values ($50\text{--}100 \text{ \AA}^2$), suggesting its rigid conformation (Figure S6B). Unlike TM11 in SERCA2b, NPTN may serve as an essential partner rather than a weakly or transiently interacting modulator of PMCA1.

Possible Mechanisms Underlying TM11-Mediated SERCA2b Regulation

The membranous domain of SERCA can be subdivided into 3 subdomains consisting of TM1–TM2, TM3–TM4, and TM5–TM10

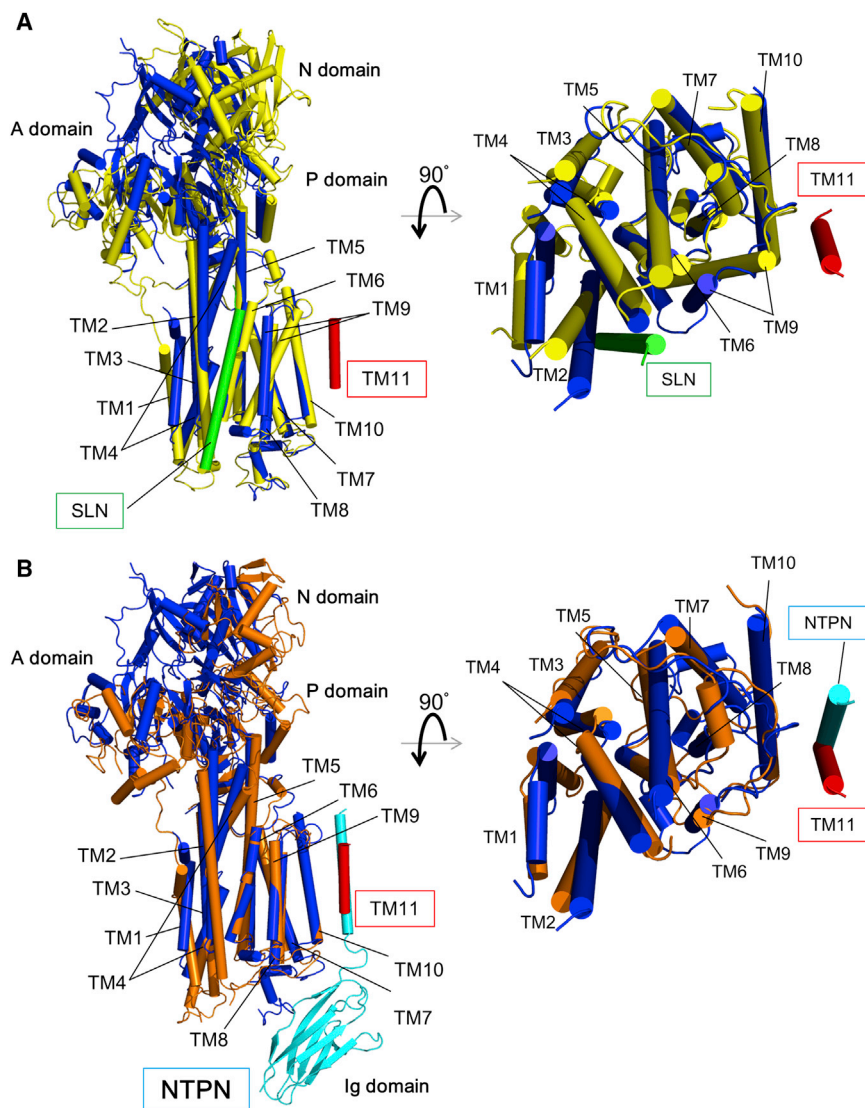


Figure 5. Positional Comparisons of the TM Helices of the Auxiliary Subunits of Ca^{2+} ATPases and TM11 in SERCA2b

(A) Crystal structures of SERCA2b in the E1- 2Ca^{2+} -AMPPCP state and sarcolipin (SLN)-bound SERCA1a in the E1- Mg^{2+} form (PBD: 3W5A) are superimposed such that the RMSD of the $\text{C}\alpha$ atoms in TM5–TM10 is minimized. SERCA2b, SERCA1a, TM11 of SERCA2b, and SLN are shown in blue, yellow, red, and green, respectively. The side view of the superimposition (left) and the top view from the cytosol (right) are shown. (B) Crystal structures of SERCA2b in the E1- 2Ca^{2+} -AMPPCP state and plasma membrane Ca^{2+} ATPase-1 (PMCA1) in complex with neuroplastin (NPTN) (PBD: 6A69) are superimposed such that the RMSD of the $\text{C}\alpha$ atoms in TM5–TM10 is minimized. SERCA2b, TM11 of SERCA2b, PMCA1, and NPTN are shown in blue, red, orange, and cyan, respectively. The side view of the superimposition (left) and the top view from the cytosol (right) are shown.

helices, respectively. During the transition between Ca^{2+} -bound E1 and Ca^{2+} -released E2 states, the association and separation of these 3 subdomains take place to control the closing and opening of the luminal Ca^{2+} pathway (Olesen et al., 2007). Concomitantly, the TM1–TM2 subdomain undergoes striking upward and downward shifts, and TM4 becomes kinked at a conserved proline residue, influencing the orientation and intra-subdomain arrangement of TM5–TM10 (Møller et al., 2010). Although no information is yet available for the structures of SERCA2b in intermediate states other than the E1- 2Ca^{2+} -AMPPCP state, it is possible that the extra TM helix weakly interacting with other TM regions serves to control such rearrangement of the TM helix bundle domain during the SERCA catalytic cycle.

In this context, when the cytosolic A, N, and P domains of SERCA2b and SERCA2a are superimposed such that the root-mean-square deviation (RMSD) of their $\text{C}\alpha$ atoms is minimized, the TM1–TM2, TM3–TM4, and TM5–TM10 subdomains of SERCA2b are shifted by 2.6° – 3.4° at the position of Ala327

with respect to those in SERCA2a, and end up further apart from TM11 as a consequence (Figure 6A). Accordingly, W1028 and V1029 of TM11 in SERCA2b would undergo steric clashes with L967, L970, and K971 of TM10 in SERCA2a (Figure 6A). To avoid these steric clashes, the movement of the TM helix bundle domain appears to be more restricted in SERCA2b than in SERCA2a (Figure 6B).

It has been established that SERCA family enzymes undergo significant dynamics in both the cytosolic and TM domains during the catalytic cycle (Møller et al., 2010). In this regard, we note that when any of the TM helix subdomains is superimposed between SERCA2a and SERCA2b, a slight but significant orientation shift is seen in their cytosolic domains, while there is no striking difference in the other TM helix subdomains (Figure S7). Thus, it is also interpretable that the presence of TM11 alters the tilt angle of the cytosolic domains relative to the TM helix bundle domain in the E1- 2Ca^{2+} -ATP state. Although structural information for other reaction intermediates is required to completely delineate how TM11 affects the location and dynamics of each TM helix and cytosolic domain during the reaction cycle, we propose a possible role for TM11 in controlling the relative arrangement of the TM helix bundle and cytosolic domains in SERCA2b for the modulation of its activity (Figure 6B).

Further Perspectives

Functional regulation by accessory TM regions has been reported previously for other P-type ATPases. In P1B-type ATPases, 2 additional N-terminal TMs modulate the entry and exit of Zn^{2+} and Cu^{2+} ions (Gourdon et al., 2011; Wang et al.,

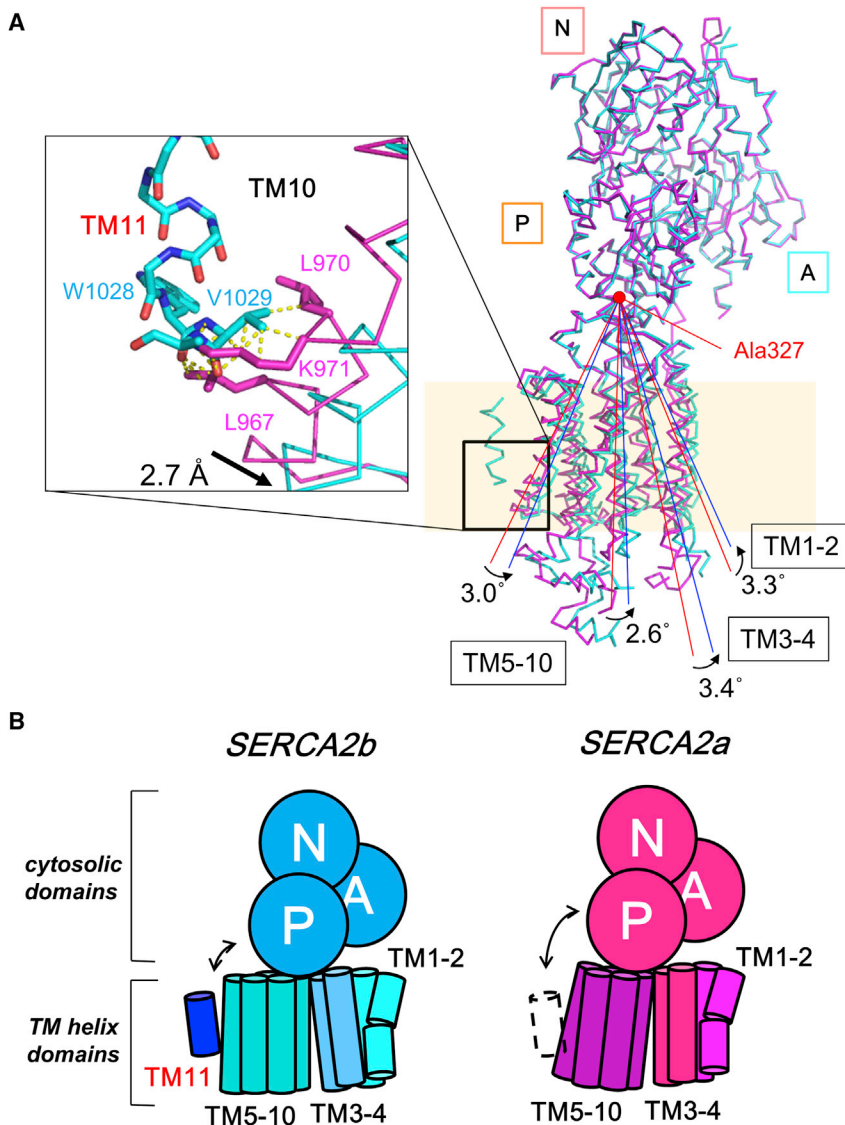


Figure 6. SERCA2b Regulation via TM11 Interplay with Other TM Helices

(A) Superposition of crystal structures of SERCA2b (cyan) and SERCA2a (magenta) highlights different tilt angles of the TM helix clusters TM1–TM2, TM3–TM4, and TM5–TM10, between the 2 proteins, in which Ala327 serves as the cardinal point. Arrows indicate that TM helices in SERCA2b are shifted by 2.6°–3.4° at the position of Ala327 with respect to those in SERCA2a, most likely due to the presence of TM11. The inset shows a close-up view of the vicinity of TM11. TM11 residues that would experience steric clashes with TM10 of SERCA2a are shown in stick representation. Yellow dotted lines in the inset indicate pairs of atoms located within 2.4 Å between TM11 of SERCA2b and TM10 of SERCA2a. (B) Proposed model of TM11-dependent regulation of the relative domain orientation in SERCA2b. The presence of TM11 restricts the movement of the TM helix bundle domain relative to the cytosolic domains due to the steric hindrance shown in (A), leading to lower ATPase activity for SERCA2b. The length of double-headed arrows reflects the mobility of the TM helices with respect to the cytosolic domains in SERCA2b (left) and SERCA2a (right).

in regulating SERCA2b activity (Li and Camacho, 2004; Marino et al., 2015; Raturi et al., 2016; Ushioda et al., 2016). While SEPN1 helps to maintain SERCA2b activity by protecting the hyperoxidation of the ER luminal Cys875 (Marino et al., 2015), the ER-resident disulfide reductase ERdj5 stimulates SERCA2b activity by reducing the Cys875–Cys887 disulfide in the L7/8 loop (Ushioda et al., 2016). ER chaperones calnexin and calreticulin and the CREC (Ca²⁺-binding protein of 45 kDa [Cab45], reticulocalbin, ER Ca²⁺-binding protein of 55 kDa [ERC-55], and calumenin) family protein Cab45S also bind SERCA2b, thereby inhibiting its Ca²⁺ pump activity

(Chen et al., 2016; John et al., 1998; Roderick et al., 2000). TMTC1 and TMTC2, which consist of multiple transmembrane segments and tetratricopeptide repeat (TPR)-containing adaptor domains, associate with SERCA2b to influence intracellular calcium levels (Sunryd et al., 2014). Thus, several ER luminal or membrane proteins are involved in the regulation of SERCA2b activity, although detailed mechanisms have yet to be uncovered. However, based on the findings of the present study, we surmise that such regulatory partner proteins may affect the location of TM11 and/or its interaction with other SERCA2b regions, thereby modulating SERCA2b activity but not SERCA2a activity. In line with this, the ER chaperone calnexin physically interacts with the C terminus of SERCA2b to control the Ca²⁺ store in the ER (Roderick et al., 2000). The structural insight gained in this study provides a framework for understanding the mechanism underlying TM11-mediated SERCA2b regulation for maintaining Ca²⁺ homeostasis in the ER.

2014). Na⁺/K⁺-ATPase forms a heterotrimer composed of an α -subunit containing A, N, and P domains, 10 TMs, and single TM β - and γ -subunits (Morth et al., 2007). Association of the β - and γ -subunits with the α -subunit modulates the affinity for K⁺ and/or Na⁺ (Geering, 2005; Hasler et al., 2001). Moreover, in the structure of H⁺-ATPase in the AMPPCP-bound state, the C-terminal regulatory domain (R domain) lacks electron density, presumably due to high flexibility (Pedersen et al., 2007). The R domain is believed to function as an auto-inhibitor that restricts TM helix movement and/or access of ions to the membrane transport core during the reaction cycle (Morth et al., 2011). Thus, regulating the interactions between additional TM moieties and the main helix bundle domain likely represents an effective and common strategy for the functional regulation of P-type ATPases.

Several recent reports suggest that ER-resident redox enzymes such as ERdj5, ERp57, TMX1, and SEPN1 are involved

(Chen et al., 2016; John et al., 1998; Roderick et al., 2000). TMTC1 and TMTC2, which consist of multiple transmembrane segments and tetratricopeptide repeat (TPR)-containing adaptor domains, associate with SERCA2b to influence intracellular calcium levels (Sunryd et al., 2014). Thus, several ER luminal or membrane proteins are involved in the regulation of SERCA2b activity, although detailed mechanisms have yet to be uncovered. However, based on the findings of the present study, we surmise that such regulatory partner proteins may affect the location of TM11 and/or its interaction with other SERCA2b regions, thereby modulating SERCA2b activity but not SERCA2a activity. In line with this, the ER chaperone calnexin physically interacts with the C terminus of SERCA2b to control the Ca²⁺ store in the ER (Roderick et al., 2000). The structural insight gained in this study provides a framework for understanding the mechanism underlying TM11-mediated SERCA2b regulation for maintaining Ca²⁺ homeostasis in the ER.

STAR★METHODS

Detailed methods are provided in the online version of this paper and include the following:

- [KEY RESOURCES TABLE](#)
- [CONTACT FOR REAGENT AND RESOURCE SHARING](#)
- [EXPERIMENTAL MODEL AND SUBJECT DETAILS](#)
- [METHOD DETAILS](#)
 - Construction of plasmids and cell lines
 - Crystallization of SERCA2b and SERCA2a
 - Data collection and structure determination
 - Preparation and analysis of SeMet-labeled SERCA2b
 - Preparation of microsomal SERCA2b and SERCA2a
 - ATPase activity assay
- [QUANTIFICATION AND STATISTICAL ANALYSIS](#)
- [DATA AND SOFTWARE AVAILABILITY](#)

SUPPLEMENTAL INFORMATION

Supplemental Information can be found online at <https://doi.org/10.1016/j.celrep.2019.03.106>.

ACKNOWLEDGMENTS

We thank the beamline scientists of SPring-8 and Photon Factory for their assistance with X-ray diffraction data collection. This work was supported by CREST, JST (to K.I. and K.N., grant number JPMJCR13M6), Grants-in-Aid for Scientific Research on Innovative Areas from MEXT (15H04335 and 26116005 to K.I. and 26119007 to T.T.), the Takeda Science Foundation (to K.I.), and the Platform Project for Supporting Drug Discovery and Life Science Research/Platform for Drug Discovery, Informatics, and Structural Life Science (PDIS) from the Japan Agency for Medical Research and Development (AMED) (to K.I.). This work was also supported by Platform Project for Supporting Drug Discovery and Life Science Research (Basis for Supporting Innovative Drug Discovery and Life Science Research [BINDS]) from AMED (JP18am0101075 and JP18am0101078 to J.T. and Y.K.).

AUTHOR CONTRIBUTIONS

M.I. constructed a large-scale expression system for SERCA2b and SERCA2a and established the purification methods. M.I. and J.T. prepared the vector for the overexpression of PA-tagged SERCA2b. N.S. purified SERCA2a on a large scale. M.I., N.S., K.Y., Y.T., and T.T. crystallized SERCA2a and SERCA2b using the LCP method. M.I., N.S., and S.W. collected and analyzed X-ray diffraction data and determined the structures of SERCA2a and SERCA2b. S.W. merged the diffraction data and refined the structures. M.I. and Y.Z. constructed plasmids for expressing SERCA2b mutants; prepared microsomal SERCA2b WT, F1019/V1028 mutants, and SERCA2a WT; and measured their ATPase activities. Y.K. prepared anti-PA antibody and conjugated Sepharose beads. K.I., R.U., and K.N. designed the study. K.I. supervised the work. M.I. and S.W. prepared the figures. K.I., M.I., and S.W. wrote the manuscript. All of the authors discussed the results and approved the manuscript.

DECLARATION OF INTERESTS

The authors declare no competing interests.

Received: December 3, 2018
Revised: February 28, 2019
Accepted: March 27, 2019
Published: April 23, 2019

REFERENCES

- Adams, P.D., Afonine, P.V., Bunkóczi, G., Chen, V.B., Davis, I.W., Echols, N., Headd, J.J., Hung, L.-W., Kapral, G.J., Grosse-Kunstleve, R.W., et al. (2010). PHENIX: a comprehensive Python-based system for macromolecular structure solution. *Acta Crystallogr. D Biol. Crystallogr.* **66**, 213–221.
- Altshuler, I., Vaillant, J.J., Xu, S., and Cristescu, M.E. (2012). The evolutionary history of sarco(endo)plasmic calcium ATPase (SERCA). *PLoS One* **7**, e52617.
- Anderson, D.M., Makarewich, C.A., Anderson, K.M., Shelton, J.M., Bezprozvannaya, S., Bassel-Duby, R., and Olson, E.N. (2016). Widespread control of calcium signaling by a family of SERCA-inhibiting micropeptides. *Sci. Signal.* **9**, ra119.
- Bai, N.C., Maurya, S.K., Sopariwala, D.H., Sahoo, S.K., Gupta, S.C., Shaikh, S.A., Pant, M., Rowland, L.A., Bombardier, E., Goonasekera, S.A., et al. (2012). Sarcolipin is a newly identified regulator of muscle-based thermogenesis in mammals. *Nat. Med.* **18**, 1575–1579.
- Burk, S.E., Lytton, J., MacLennan, D.H., and Shull, G.E. (1989). cDNA Cloning, Functional Expression, and mRNA Tissue Distribution of a Third Organellar Ca²⁺ Pump. *J. Biol. Chem.* **264**, 18561–18566.
- Caffrey, M., and Cherezov, V. (2009). Crystallizing membrane proteins using lipidic mesophases. *Nat. Protoc.* **4**, 706–731.
- Campbell, A.M., Kessler, P.D., Sagara, Y., Inesi, G., and Fambrough, D.M. (1991). Nucleotide sequences of avian cardiac and brain SR/ER Ca²⁺-ATPases and functional comparisons with fast twitch Ca²⁺-ATPase. Calcium affinities and inhibitor effects. *J. Biol. Chem.* **266**, 16050–16055.
- Campbell, A.M., Kessler, P.D., and Fambrough, D.M. (1992). The alternative carboxyl termini of avian cardiac and brain sarcoplasmic reticulum/endo-plasmic reticulum Ca²⁺-ATPases are on opposite sides of the membrane. *J. Biol. Chem.* **267**, 9321–9325.
- Chen, L., Xu, S., Xu, Y., Lu, W., Liu, L., Yue, D., Teng, J., and Chen, J. (2016). Cab45S promotes cell proliferation through SERCA2b inhibition and Ca signaling. *Oncogene* **35**, 35–46.
- Clausen, J.D., Vandecaetsbeek, I., Wuytack, F., Vangheluwe, P., and Andersen, J.P. (2012). Distinct roles of the C-terminal 11th transmembrane helix and luminal extension in the partial reactions determining the high Ca²⁺ affinity of sarco(endo)plasmic reticulum Ca²⁺-ATPase isoform 2b (SERCA2b). *J. Biol. Chem.* **287**, 39460–39469.
- De Lano, W.L. (2006). The PyMol Molecular Graphics System (De Lano Scientific, LLC).
- Dode, L., Andersen, J.P., Leslie, N., Dhitavat, J., Vilsen, B., and Hovnanian, A. (2003). Dissection of the functional differences between sarco(endo)plasmic reticulum Ca²⁺-ATPase (SERCA) 1 and 2 isoforms and characterization of Darier disease (SERCA2) mutants by steady-state and transient kinetic analyses. *J. Biol. Chem.* **278**, 47877–47889.
- Emsley, P., and Cowtan, K. (2004). Coot: model-building tools for molecular graphics. *Acta Crystallogr. D Biol. Crystallogr.* **60**, 2126–2132.
- Emsley, P., Lohkamp, B., Scott, W.G., and Cowtan, K. (2010). Features and development of Coot. *Acta Crystallogr. D Biol. Crystallogr.* **66**, 486–501.
- Evans, P.R., and Murshudov, G.N. (2013). How good are my data and what is the resolution? *Acta Crystallogr. D Biol. Crystallogr.* **69**, 1204–1214.
- Fujii, Y., Matsunaga, Y., Arimori, T., Kitago, Y., Ogasawara, S., Kaneko, M.K., Kato, Y., and Takagi, J. (2016). Tailored placement of a turn-forming PA tag into the structured domain of a protein to probe its conformational state. *J. Cell Sci.* **129**, 1512–1522.
- Geering, K. (2005). Function of FXYD proteins, regulators of Na, K-ATPase. *J. Bioenerg. Biomembr.* **37**, 387–392.
- Gong, D., Chi, X., Ren, K., Huang, G., Zhou, G., Yan, N., Lei, J., and Zhou, Q. (2018). Structure of the human plasma membrane Ca²⁺-ATPase 1 in complex with its obligatory subunit neuroplastin. *Nat. Commun.* **9**, 3623.
- Gorski, P.A., Trieber, C.A., Larivière, E., Schuermans, M., Wuytack, F., Young, H.S., and Vangheluwe, P. (2012). Transmembrane helix 11 is a genuine regulator of the endoplasmic reticulum Ca²⁺ pump and acts as a functional parallel of β -subunit on α -Na⁺,K⁺-ATPase. *J. Biol. Chem.* **287**, 19876–19885.

- Gourdon, P., Liu, X.Y., Skjorringe, T., Morth, J.P., Møller, L.B., Pedersen, B.P., and Nissen, P. (2011). Crystal structure of a copper-transporting PIB-type ATPase. *Nature* 475, 59–64.
- Hasler, U., Crambert, G., Horisberger, J.D., and Geering, K. (2001). Structural and functional features of the transmembrane domain of the Na,K-ATPase beta subunit revealed by tryptophan scanning. *J. Biol. Chem.* 276, 16356–16364.
- Hughes, G., East, J.M., and Lee, A.G. (1994). The hydrophilic domain of phospholamban inhibits the Ca²⁺ transport step of the Ca(2+)-ATPase. *Biochem. J.* 303, 511–516.
- Ikedo, K., Kang, Q., Yoneshiro, T., Camporez, J.P., Maki, H., Homma, M., Shinoda, K., Chen, Y., Lu, X., Maretich, P., et al. (2017). UCP1-independent signaling involving SERCA2b-mediated calcium cycling regulates beige fat thermogenesis and systemic glucose homeostasis. *Nat. Med.* 23, 1454–1465.
- Inaba, K., Murakami, S., Suzuki, M., Nakagawa, A., Yamashita, E., Okada, K., and Ito, K. (2006). Crystal structure of the DsbB-DsbA complex reveals a mechanism of disulfide bond generation. *Cell* 127, 789–801.
- Inaba, K., Murakami, S., Nakagawa, A., Iida, H., Kinjo, M., Ito, K., and Suzuki, M. (2009). Dynamic nature of disulfide bond formation catalysts revealed by crystal structures of DsbB. *EMBO J.* 28, 779–791.
- John, L.M., Lechleiter, J.D., and Camacho, P. (1998). Differential modulation of SERCA2 isoforms by calreticulin. *J. Cell Biol.* 142, 963–973.
- Kabsch, W. (2010). XDS. *Acta Crystallogr. D Biol. Crystallogr.* 66, 125–132.
- Li, Y., and Camacho, P. (2004). Ca²⁺-dependent redox modulation of SERCA 2b by ERp57. *J. Cell Biol.* 164, 35–46.
- MacLennan, D.H., and Kranias, E.G. (2003). Phospholamban: a crucial regulator of cardiac contractility. *Nat. Rev. Mol. Cell Biol.* 4, 566–577.
- Marino, M., Stoilova, T., Giorgi, C., Bachi, A., Cattaneo, A., Auricchio, A., Pinton, P., and Zito, E. (2015). SEP11, an endoplasmic reticulum-localized selenoprotein linked to skeletal muscle pathology, counteracts hyperoxidation by means of redox-regulating SERCA2 pump activity. *Hum. Mol. Genet.* 24, 1843–1855.
- Mikkelsen, S.A., Vangheluwe, P., and Andersen, J.P. (2018). A Darier disease mutation relieves kinetic constraints imposed by the tail of sarco(endo)plasmic reticulum Ca(2+)-ATPase 2b. *J. Biol. Chem.* 293, 3880–3889.
- Møller, J.V., Olesen, C., Winther, A.M., and Nissen, P. (2010). The sarco-plasmic Ca²⁺-ATPase: design of a perfect chemi-osmotic pump. *Q. Rev. Biophys.* 43, 501–566.
- Morth, J.P., Pedersen, B.P., Toustrup-Jensen, M.S., Sørensen, T.L., Petersen, J., Andersen, J.P., Vilsen, B., and Nissen, P. (2007). Crystal structure of the sodium-potassium pump. *Nature* 450, 1043–1049.
- Morth, J.P., Pedersen, B.P., Buch-Pedersen, M.J., Andersen, J.P., Vilsen, B., Palmgren, M.G., and Nissen, P. (2011). A structural overview of the plasma membrane Na⁺,K⁺-ATPase and H⁺-ATPase ion pumps. *Nat. Rev. Mol. Cell Biol.* 12, 60–70.
- Odermatt, A., Becker, S., Khanna, V.K., Kurzydowski, K., Leisner, E., Pettei, D., and MacLennan, D.H. (1998). Sarcolipin Regulates the Activity of SERCA1, the Fast-twitch Skeletal Muscle Sarcoplasmic Reticulum Ca²⁺-ATPase. *J. Biol. Chem.* 273, 12360–12369.
- Olesen, C., Picard, M., Winther, A.M., Gyrop, C., Morth, J.P., Oxvig, C., Møller, J.V., and Nissen, P. (2007). The structural basis of calcium transport by the calcium pump. *Nature* 450, 1036–1042.
- Pedersen, B.P., Buch-Pedersen, M.J., Morth, J.P., Palmgren, M.G., and Nissen, P. (2007). Crystal structure of the plasma membrane proton pump. *Nature* 450, 1111–1114.
- Raturi, A., Gutiérrez, T., Ortiz-Sandoval, C., Ruangkittisakul, A., Herrera-Cruz, M.S., Rockley, J.P., Gesson, K., Ourdev, D., Lou, P.H., Lucchinetti, E., et al. (2016). TMX1 determines cancer cell metabolism as a thiol-based modulator of ER-mitochondria Ca²⁺ flux. *J. Cell Biol.* 214, 433–444.
- Roderick, H.L., Lechleiter, J.D., and Camacho, P. (2000). Cytosolic phosphorylation of calnexin controls intracellular Ca(2+) oscillations via an interaction with SERCA2b. *J. Cell Biol.* 149, 1235–1248.
- Schmidt, N., Kollwe, A., Constantin, C.E., Henrich, S., Ritzau-Jost, A., Bildl, W., Saalbach, A., Hallermann, S., Kulik, A., Fakler, B., and Schulte, U. (2017). Neuroplastin and Basigin Are Essential Auxiliary Subunits of Plasma Membrane Ca²⁺-ATPases and Key Regulators of Ca²⁺ Clearance. *Neuron* 96, 827–838.e9.
- Schoenmakers, T.J., Visser, G.J., Flik, G., and Theuvsen, A.P. (1992). CHELATOR: an improved method for computing metal ion concentrations in physiological solutions. *Biotechniques* 12, 870–874, 876–879.
- Sitsel, A., De Raeymaecker, J., Drachmann, N.D., Derua, R., Smaardijk, S., Andersen, J.L., Vandecaetsbeek, I., Chen, J., De Maeyer, M., Waelkens, E., et al. (2019). Structures of the heart specific SERCA2a Ca(2+)-ATPase. *EMBO J.* Published online February 18, 2019. <https://doi.org/10.15252/emboj.2018100020>.
- Sørensen, T.L.-M., Møller, J.V., and Nissen, P. (2004). Phosphoryl transfer and calcium ion occlusion in the calcium pump. *Science* 304, 1672–1675.
- Sunryd, J.C., Cheon, B., Graham, J.B., Giorda, K.M., Fissore, R.A., and Hebert, D.N. (2014). TMTC1 and TMTC2 are novel endoplasmic reticulum tetrapeptide repeat-containing adapter proteins involved in calcium homeostasis. *J. Biol. Chem.* 289, 16085–16099.
- Toyoshima, C., and Mizutani, T. (2004). Crystal structure of the calcium pump with a bound ATP analogue. *Nature* 430, 529–535.
- Toyoshima, C., Asahi, M., Sugita, Y., Khanna, R., Tsuda, T., and MacLennan, D.H. (2003). Modeling of the inhibitory interaction of phospholamban with the Ca²⁺ ATPase. *Proc. Natl. Acad. Sci. USA* 100, 467–472.
- Toyoshima, C., Iwasawa, S., Ogawa, H., Hirata, A., Tsueda, J., and Inesi, G. (2013). Crystal structures of the calcium pump and sarcolipin in the Mg²⁺-bound E1 state. *Nature* 495, 260–264.
- Ushioda, R., Miyamoto, A., Inoue, M., Watanabe, S., Okumura, M., Maegawa, K.I., Uegaki, K., Fujii, S., Fukuda, Y., Umitsu, M., et al. (2016). Redox-assisted regulation of Ca²⁺ homeostasis in the endoplasmic reticulum by disulfide reductase ERdj5. *Proc. Natl. Acad. Sci. USA* 113, E6055–E6063.
- Vagin, A., and Teplyakov, A. (2010). Molecular replacement with MOLREP. *Acta Crystallogr. D Biol. Crystallogr.* 66, 22–25.
- Vandecaetsbeek, I., Trekels, M., De Maeyer, M., Ceulemans, H., Lescrinier, E., Raeymaekers, L., Wuytack, F., and Vangheluwe, P. (2009). Structural basis for the high Ca²⁺ affinity of the ubiquitous SERCA2b Ca²⁺ pump. *Proc. Natl. Acad. Sci. USA* 106, 18533–18538.
- Verboomen, H., Wuytack, F., De Smedt, H., Himpens, B., and Casteels, R. (1992). Functional difference between SERCA2a and SERCA2b Ca²⁺ pumps and their modulation by phospholamban. *Biochem. J.* 286, 591–595.
- Verboomen, H., Wuytack, F., Van den Bosch, L., Mertens, L., and Casteels, R. (1994). The functional importance of the extreme C-terminal tail in the gene 2 organellar Ca(2+)-transport ATPase (SERCA2a/b). *Biochem. J.* 303, 979–984.
- Wang, K., Sitsel, O., Meloni, G., Autzen, H.E., Andersson, M., Klymchuk, T., Nielsen, A.M., Rees, D.C., Nissen, P., and Gourdon, P. (2014). Structure and mechanism of Zn²⁺-transporting P-type ATPases. *Nature* 514, 518–522.
- Waterman, D.G., Winter, G., Gildea, R.J., Parkhurst, J.M., Brewster, A.S., Sauter, N.K., and Evans, G. (2016). Diffraction-geometry refinement in the DIALS framework. *Acta Crystallogr. D Struct. Biol.* 72, 558–575.
- Winther, A.-M.L., Bublitz, M., Karlson, J.L., Møller, J.V., Hansen, J.B., Nissen, P., and Buch-Pedersen, M.J. (2013). The sarcolipin-bound calcium pump stabilizes calcium sites exposed to the cytoplasm. *Nature* 495, 265–269.
- Yamashita, K., Hirata, K., and Yamamoto, M. (2018). KAMO: towards automated data processing for microcrystals. *Acta Crystallogr. D Struct. Biol.* 74, 441–449.

STAR★METHODS

KEY RESOURCES TABLE

REAGENT or RESOURCE	SOURCE	IDENTIFIER
Antibodies		
SERCA2 Antibody (N-19)	Santa Cruz Biotechnology	sc-8095
Donkey F(ab') ₂ Anti-Goat IgG (HRP)	Abcam	Ab98519
Chemicals, Peptides, and Recombinant Proteins		
Cumate (p-Isopropylbenzoic Acid)	FUJIFILM Wako Pure Chemical Corporation	037-06412
Phorbol 12-myristate 13-acetate	FUJIFILM Wako Pure Chemical Corporation	168-23593
Monoolein	Nu-Chek-Prep, Inc.	M-239
β, γ -Methyleneadenosine 5' -triphosphate disodium salt	Sigma	M7510
Polyethylenimine	Sigma	408727
Seleno-L-methionine	NACALAI TESQUE	02286-75
PA-SERCA2b	Ushioda et al., 2016	N/A
PA-SERCA2a	This study	N/A
Critical Commercial Assays		
EnzCheck™ Phosphate Assay Kit	Thermo Fisher Scientific	E6646
Deposited Data		
SERCA2b E1-AMPPCP form	This paper	PDB: 5ZTF
SERCA2a E1-AMPPCP form	This paper	PDB: 6JJU
Experimental Models: Cell Lines		
Human: HEK293T cells	ATCC	CRL-3216
Oligonucleotides		
Primer: SERCA2a forward: taatacgactcactataggg	This paper	N/A
Primer: SERCA2a reverse: tgcggccgcttactccagta ttgcaggtccaggtagttgctggcc	This paper	N/A
Primer: SERCA2bF1018G forward: taccctaaagga ccggccacacgacgagtattac	This paper	N/A
Primer: SERCA2bF1018G reverse: forward:catta tgagcagcacaccggccaggaatcccat	This paper	N/A
Primer: SERCA2bV1029G forward: cggggaccact agacccaatatcgtgtctgtgat	This paper	N/A
Primer: SERCA2bV1029G reverse: tagtgtctgtgct ataacccagatcaccaggggc	This paper	N/A
Recombinant DNA		
Plasmid: pcDNA3.1/PA-SERCA2b	Ushioda et al., 2016	N/A
PiggyBac Cumate Switch Inducible Vector	System Biosciences, LLC, CA, USA	#PBQM812A-1
Super PiggyBac Transposase Expression Vector	System Biosciences, LLC, CA, USA	#PB200PA-1
Software and Algorithms		
Prism 7	GraphPad software	N/A
XDS	Kabsch, 2010	http://xds.mpimf-heidelberg.mpg.de
KAMO	Yamashita et al., 2018	N/A
DIALS	Waterman et al., 2016	N/A
MOLREP	Vagin and Teplyakov, 2010	http://www.ccp4.ac.uk/html/molrep.html

(Continued on next page)

Continued

REAGENT or RESOURCE	SOURCE	IDENTIFIER
AIMLESS	Evans and Murshudov, 2013	N/A
Image Lab	Bio-Rad Laboratories, Inc., CA, USA	N/A
COOT	Emsley and Cowtan, 2004	https://www2.mrc-lmb.cam.ac.uk/personal/pemsley/coot/
PHENIX	Adams et al., 2010	https://www.phenix-online.org
Pymol	De Lano, 2006	https://pymol.org/2/

CONTACT FOR REAGENT AND RESOURCE SHARING

Further information and requests for resources and reagents should be directed to and will be fulfilled by the Lead Contact, Kenji Inaba (kinaba@tagen.tohoku.ac.jp).

EXPERIMENTAL MODEL AND SUBJECT DETAILS

HEK293T cells were used for overexpression of recombinant human SERCA2b and SERCA2a.

METHOD DETAILS**Construction of plasmids and cell lines**

In the present crystallographic studies, we engineered PA-tagged SERCA2a (PA-SERCA2a) using plasmid pcDNA3.1/PA-SERCA2b constructed in our previous study ([Ushioda et al., 2016](#)) as a template. The open reading frame (ORF) of SERCA2a was amplified by PCR using primers 5'-taatacagactactataggg-3' and 5'-tgcggccgcttactccagtagtccaggttccaggttagtgcgggcc-3' and subcloned into pcDNA3.1. The ORF of PA-SERCA2b or PA-SERCA2a was isolated from pcDNA3.1 by digestion with *NheI* and *NotI*, and inserted into the *NheI* and *NotI* sites of the PiggyBac Cumate Switch Inducible Vector (System Biosciences, LLC, CA, USA) to establish a cell line that inducibly expresses PA-SERCA2b or PA-SERCA2a, respectively. For functional assays, we also engineered the F1018G, V1029G and F1018G/V1029G mutants of PA-SERCA2b using the plasmid pcDNA3.1/PA-SERCA2b as a template. The SERCA2b mutants were prepared by site-directed mutagenesis with appropriate primers as follows: 5'-taccctaaaggaccggccacacgacgagtattac-3' and 5'-cattatgagcagcacacccggccaggaatcccat-3' for F1018G, 5'-cggggaccactagaccccaaatatcgtgtctgtgat-3' and 5'-tagtctgtgtctataaccccgatcaccaggggc-3' for V1029G and the all four primers for F1018G/V1029G.

Crystallization of SERCA2b and SERCA2a

Expression and purification of PA-SERCA2b and PA-SERCA2a were performed as described previously ([Ushioda et al., 2016](#)), except that 1 mM sodium butyrate was not included in induction reagents. Briefly, HEK293T cells were co-transfected with the PA-SERCA2b- or PA-SERCA2a-inserted PiggyBac Cumate Switch Inducible vector and Super PiggyBac Transposase Expression Vector (System Biosciences, LLC, CA, USA) using polyethylenimine (Sigma) to establish a cell line stably expressing each of the proteins. High expressions of PA-SERCA2b and HA-SERCA2a were induced with cumate and 50 ng/ml phorbol 12-myristate 13-acetate (PMA). The cells were cultured in DMEM supplemented with 4% inactivated fetal calf serum at 37°C for 48 hr after induction. Harvested cells were solubilized with 1% (w/v) DDM, and PA-SERCA2b and PA-SERCA2a were purified by anti-PA Sepharose beads. During the final step of purification, PA-SERCA2b and PA-SERCA2a were passed through a Superose 6 column (GE Healthcare UK Ltd., Buckinghamshire, UK) equilibrated with buffer containing 100 mM MOPS (pH 6.8), 80 mM KCl, 20% glycerol, 1 mM CaCl₂, 1 mM MgCl₂, 1 mM DTT and 0.1% n-dodecyl-β-D-maltoside (DDM). PA-SERCA2b and PA-SERCA2a thus purified were concentrated to 10–18 mg ml⁻¹, mixed with 1 mM AMPPCP and incubated overnight at 4°C. After centrifugation at 22,300 g for 30 min, proteins were reconstituted into monoolein at a protein-to-lipid ratio of 2:3 (v/v) ([Caffrey and Cherezov, 2009](#)). Crystals of PA-SERCA2b were grown at 20°C in reservoir solution (28–34% polyethylene glycol 250 dimethylethanol, 100 mM Tris-HCl (pH 7.1–7.3), 100 mM KSCN) for 2–3 days. Similarly, crystals of PA-SERCA2a were grown at 16°C in 28.5–29.5% polyethylene glycol 250 dimethylethanol, 100 mM Tris-HCl (pH 7.7) and 50 mM NH₄NO₃ for 2–3 days.

Data collection and structure determination

X-ray diffraction data were collected at SPring-8 beamline BL32XU. Small wedges of data were collected from a number of micro-crystals and scaled together. For reduced SERCA2a, a complete dataset was collected from a single crystal. Diffraction data were integrated with XDS ([Kabsch, 2010](#)) using the KAMO system ([Yamashita et al., 2018](#)) or DIALS ([Waterman et al., 2016](#)). Multiple datasets were analyzed with BLEND, followed by scaling and merging with AIMLESS ([Evans and Murshudov, 2013](#)) based on CC_{1/2} values. Initial phases were calculated by molecular replacement with MOLREP using the rabbit SERCA1a E1-AMPPCP structure

(PBD ID: 1T5S). Model building and refinement were carried out with COOT (Emsley et al., 2010) and PHENIX (Adams et al., 2010), respectively. Final models were refined to reasonable R_{free} values with good geometry, compared with all published crystal structures of comparable resolution.

Preparation and analysis of SeMet-labeled SERCA2b

Cells inducibly expressing PA-SERCA2b were cultured in 4% FCS and Dulbecco's modified Eagles' medium (DMEM) without methionine. Expression of SeMet-labeled PA-SERCA2b was induced with 30 $\mu\text{g/ml}$ Seleno-L-methionine, 50 nM phorbol 12-myristate 13-acetate and 150 $\mu\text{g/ml}$ cumate. Cells were harvested after 2 days of incubation at 37°C. Purification, crystallization and X-ray diffraction data collection for SeMet-labeled SERCA2b were performed following the same procedures as described above, except that radiation with a wavelength of 0.978 Å was employed for data collection and calculation of an anomalous difference Fourier map to identify SeMet residues in SERCA2b.

Preparation of microsomal SERCA2b and SERCA2a

HEK293T cells transfected with WT, F1018G, V1029G or F1018G/V1029G mutants of PA-SERCA2b or WT PA-SERCA2a were incubated in DMEM at 37°C for 2 days. Harvested cells were repeatedly homogenized in 250 mM sucrose, 150 mM KCl, 10 mM Tris-HCl (pH 7.5), 100 nM CaCl_2 and 0.2% NaN_3 with a Dounce Tissue Grinder (DWK Life Sciences GmbH, Wertheim/Main, Germany), and subsequently centrifuged at 10,000 g for 20 min at 4°C. Homogenates were ultracentrifuged at 100,000 g for 1 hour at 4°C, and pellets were resuspended in 50 mM HEPES (pH 7.0), 100 mM NaCl and 20% glycerol, and homogenized by repeatedly passing the suspension through a 1 mL syringe with a 25 G needle. The concentrations of SERCA2b and SERCA2a in microsomes were estimated by western blotting with anti-SERCA2 antibody, based on a calibration curve calculated from the band intensity of purified SERCA2b of known concentrations. Band intensities were quantified and analyzed by Image Lab (Bio-Rad Laboratories, Inc., CA, USA).

ATPase activity assay

The ATPase activities of SERCA2b and SERCA2a in microsomes were measured as described previously (Ushioda et al., 2016). Briefly, the microsomal SERCA2b or SERCA2a was incubated in buffer containing 50 mM HEPES (pH 7.0), 100 mM NaCl, 20% glycerol, 50 mM NaN_3 , 5 mM MgCl_2 , 1 mM EGTA and various concentrations of CaCl_2 . 1 mM ATP was added to initiate the SERCA ATPase cycle. Each calcium concentration in the reaction buffer was determined using the chelator program (Schoenmakers et al., 1992). The reaction was stopped by 5 mM EGTA, and the resultant solution was mixed with EnzCheck phosphate assay kit (Thermo Fisher Scientific). The mixture was incubated at 22°C for 30 min, and the absorbance at 360 nm was measured by U-3900 Spectrophotometer (HITACHI). Curve fitting of the SERCA2b and SERCA2a activities at different calcium concentrations was performed using Prism7 (Graphpad software) to determine K_d for Ca^{2+} , V_{max} and Hill slope values (Table S1).

QUANTIFICATION AND STATISTICAL ANALYSIS

Biochemical assays shown in Figure 4 were performed in three independent replicates. Statistical analysis was performed in GraphPad Prism7 using one-way ANOVA analysis followed by Tukey's multiple comparison test. Values are expressed as means \pm SD. Differences with a p -value of < 0.05 are considered to be significant.

DATA AND SOFTWARE AVAILABILITY

Atomic coordinates and structure factors of human SERCA2b and SERCA2a have been deposited in the Protein Data Bank under accession codes 5ZTF and 6JJU, respectively.